

## Phase effect in the energy loss of hydrogen projectiles in zinc targets

A. Arnau

*Departamento de Física de Materiales, Universidad del País Vasco, Apartado 1072, 20080 San Sebastian, Spain*

P. Bauer and F. Kastner

*Institut für Experimentalphysik, Johannes Kepler Universität, A-4040 Linz, Austria*

A. Salin

*Laboratoire des Collisions Atomiques, Centre National de la Recherche Scientifique et Université Bordeaux I, 351 Cours de la Libération, 33405 Talence Cedex, France*

V. H. Ponce and P. D. Fainstein

*Centro Atómico Bariloche and Instituto Balseiro, 8400 Bariloche, Argentina*

P. M. Echenique

*Departamento de Física de Materiales, Universidad del País Vasco, Apartado 1072, 20080 San Sebastian, Spain*

(Received 14 July 1993; revised manuscript received 1 November 1993)

We present an experimental and theoretical study of the phase effect in the energy loss of fast hydrogen beams colliding with gas and solid zinc targets. The experiments show a maximum phase effect of 50% around 50 keV/u, the energy loss per atom in the solid target being smaller than in the gas target. An extensive theoretical study of all the processes contributing to the energy loss in the two phases shows that the experimental findings can be explained primarily by the screening of the projectile field by the valence electrons in the solid.

### I. INTRODUCTION

The energy loss (stopping) of atomic particles traversing matter is a phenomenon relevant to many fields of pure and applied physics. Advances in the comprehension of this subject have been tied to a successful description of the response of atomic<sup>1</sup> and solid-state<sup>2</sup> systems to external perturbations. On the experimental side, the numerous studies on a large number of projectile, target, and energy combinations<sup>3</sup> can, nevertheless, only cover a small fraction of the systems and energies of relevance for areas as varied as nuclear, solid state, plasma, and medical physics. Understanding the dependence of energy loss on the nature of the target acquires, then, a practical importance: to predict the stopping of many targets from formalisms tested with measurements on a small number of them.

Let us assume that we can describe, and have checked with measurements, the stopping of targets made of pure elements in the gas phase. To predict the stopping produced by any compound target for the same kind of projectile, it would be necessary to know the effect on stopping of chemical binding and of the state of aggregation (phase) of the target. These so-called "chemical" and "phase" effects can be described more easily in the high velocity limit of stopping. By high velocities we mean those for which the projectile has no bound electrons on the average, so that the inelastic processes that produce the stopping are of the simplest type: target excitations (including ionization) by a bare charge. Summation over final states produces the Bethe formula for stopping,

where the dependence on the projectile charge  $Z_1$  appears as a factor  $Z_1^2$  and on the target through  $Z_2$ , target atomic number, and a logarithmic term thus producing a weak dependence on the target parameters. At high velocities excitation of the target inner shells contributes to the energy loss, so that, for target atomic numbers  $Z_2 > 10$ , the contribution of valence electrons to stopping is a small fraction of the total. Since only the valence electron state is changed when going from isolated atoms to molecular or solid complexes, we may assert that the stopping in a compound system is the average of the stopping for the pure elements weighted by the relative number of atoms of each element entering the compound. This is Bragg's rule, frequently used in the estimation of stopping.<sup>4,5</sup> As we have indicated, it is valid at high velocities and for heavy target atoms.

We now analyze the ways in which Bragg's rule ceases to be valid at medium energies, i.e., those where the maximum in the stopping is attained. Since in this range valence electrons are responsible for the main part of the stopping, this is an obvious reason for the breakdown of the rule. But, if this were the only reason, then the remedy would be at hand: The stopping by valence electrons should be calculated by accounting for the changes they undergo to produce the chemical bonds of the molecule or the solid. This correction has already been attempted,<sup>6</sup> taking semiphenomenological parameters to quantify the valence electron states in the compound, and using them in a generalized form of Bethe's formula. Unfortunately, measurements show agreement with calculations in some cases and none in others.<sup>5,7</sup> The main

reason is that Bethe's formula is out of its range of validity at medium energies. The assumption of the projectile acting exclusively as a bare charge is no longer valid: When the projectile velocity is close to the typical one for the target valence electrons, the electron capture and projectile ionization cross sections have the same order of magnitude and there will be a statistical distribution of projectile charge states. Furthermore, for a given charge state there will be a distribution in the population of bound states of the ion. At asymptotically high velocities the projectile charge-state fractions are zero except for the bare nucleus. At velocities where other charge fractions become appreciable, the description of bound states on the projectile is far from trivial when dealing with a solid target: Screening by target electrons will reduce the binding and a finite energy width will represent the collisional destruction of the state.<sup>8</sup>

The statistical distribution over projectile charge states destroys the  $Z_1^2$  dependence of Bethe's formula. Each charge state, and even each possible projectile state, will contribute to stopping with its statistical weight. To recover the simplicity of a structureless projectile, effective charge models<sup>9</sup> consider the projectile as a bare ion with charge equal to the average of the projectile charge. Due to the strong dependence of transition amplitudes on the internal degrees of freedom of the projectile ion (it is not at all the same to excite a target or capture an electron by a bare charge of value 0.5 than with 50% of protons and 50% of neutral hydrogen atoms), this model cannot describe chemical or phase effects on stopping. Furthermore, the presence of bound projectile states opens up new mechanisms for energy-loss like projectile excitation and simultaneous target and projectile excitation. Finally, the very existence of a charge distribution proves the importance of electron capture and projectile ionization, since it is their combined action which determines the projectile charge-state fractions.

In this work we study the difference in electronic stopping cross section between a metallic element in the gaseous and solid forms. The motivation of this paper is to present a systematic study of all the factors that determine the phase effect in stopping. To our knowledge, the only previous experimental study of the phase effect in a metallic element is the work of Meckbach and Allison,<sup>10</sup> where the relative stopping between  $\text{He}^+$  and  $\text{H}^+$  ions in

vapor and metal Cd target was measured. It is therefore of fundamental importance to perform absolute measurements in a well controlled target system, over a range of energies that covers the stopping power maximum. We have chosen Zn as the target element due to the highly controlled conditions in which vapor and solid films can be prepared. Measurements of stopping have been performed for H projectiles in the energy range 15–720 keV/u. These are presented in Sec. II and show a remarkable phase effect. In Secs. III and IV we analyze the mechanisms that produce the phase effect, using approximations for valence electrons that are appropriate for the pure atomic transition processes in the gas phase or the collective response of the metal. In the gas phase we use first-order approximations to transitions where the target and projectile are excited. We consider a distorted-wave approximation for projectile capture. For the solid we use a free-electron gas description of the 4s electrons, and atomic orbitals for the 3d subshell. The electron bound state around the proton is described through the self-consistent linear response model,<sup>8</sup> and the capture and loss transitions are described as three-body recombinations-type processes with simultaneous single particle or collective excitation in the electron gas.<sup>11</sup> The description of the solid stopping along these premises is also justified at low velocities, and gives, in principle, a correct description of the stopping on both sides of the stopping maximum. A brief account of this work has already been presented.<sup>12</sup>

## II. EXPERIMENT

The experiment was performed at the University of Linz using the 700-keV Van de Graaff accelerator.

### A. Experimental setup

A schematic drawing of the experimental setup is shown in Fig. 1. It consists of the *vapor chamber* containing the vapor cell that includes provisions for heating and for temperature measurement, the *deflection chamber* containing the deflection unit and the condensation baffles, and the *scattering chamber* with additional shielding baffles, the target manipulator, and the detector system. For energy-loss measurements, a vapor cell is supe-

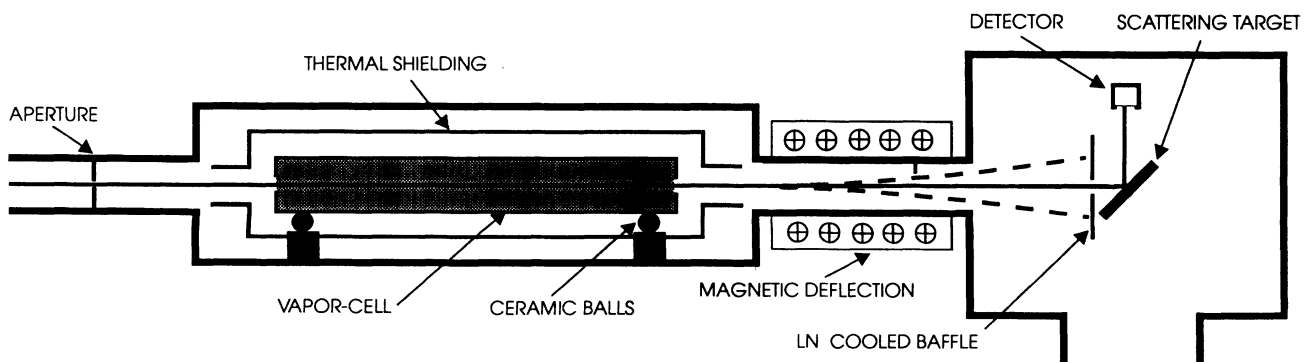


FIG. 1. Schematic representation of the experimental setup.

rior to an atomic beam because rather high atomic densities are needed. In our experiment, the range of areal densities is  $3 \times 10^{16}/\text{cm}^2$  to  $2 \times 10^{17}/\text{cm}^2$ .

Because of the high temperatures in the vapor cell the vapor chamber is metal sealed. Under measuring conditions, the whole vacuum system is operated in the  $10^{-8}$  mbar range. The layout of the individual chambers is such that, despite of the high vapor densities in the vapor cell, no zinc is deposited on sensitive parts of the apparatus.

The vapor cell has a length of 30 cm and is made of stainless steel. Thus, despite of the reactivity of zinc at temperatures of 500 °C, chemical reactions with the vapor cell are minimized. Because of the rather low thermal conductivity of steel, special care was taken to achieve a homogeneous temperature distribution along the vapor cell. Nevertheless, a temperature difference of several Kelvin between the center and the ends of the cell remained. The temperature measurements were performed by means of Fe-Constantan thermocouples positioned at different points of the vapor cell. Thermal shielding was applied around the vapor cell in order to minimize the heating power and to obtain time constants as large as possible. Thus, it was easy to keep the temperature during a measurement constant within  $\pm 0.3^\circ\text{C}$ , which corresponds to a stability of  $< 1\%$  for the vapor pressure. In the cell, the zinc vapor was in thermal equilibrium with the condensed phase (usually the liquid). Because of the low dissociation energy of  $\text{Zn}_2$ , the dimer content is negligible.<sup>13</sup>

The apertures of the vapor cell have a diameter of 1.5 mm and are not covered by sealing foils. Thus, the measurement of the energy loss is more precise, as only metal vapor contributes, and the intensity of the transmitted ions is higher, as it is not decreased by multiple scattering in the foils.<sup>14</sup> On the other hand, effusion of the vapor causes an increase in the effective length of the vapor cell which must be taken into account in a precise absolute measurement and it may cause problems because of the condensates deposited in the cooler parts of the setup. The temperature of the apertures could be varied by heating them separately from the vapor cell itself. Therefore, it was possible to avoid condensation of zinc in the region of the apertures. By mounting the vapor cell on one conus and on two perpendicular grooves via ceramic spheres it was possible to allow for thermal expansion (up to 3 mm) without losing the mechanical adjustment relative to the ion beam up to temperatures of 600 °C.

The *deflection chamber* is situated downstream of the vapor chamber. In this region, a homogeneous magnetic field may be applied perpendicularly to the ion beam. With the magnetic field applied, the ions are separated according to their charge states after having left the vapor cell. Thus, the charge state of the ions impinging on the scattering target can be chosen.

In the *scattering chamber*, there are shielding baffles which are cooled by a liquid-nitrogen trap. These shielding baffles act as predominant places of vapor condensation due to the temperature dependence of the sticking probability. The target manipulator holds up to six targets and permits a linear motion to select the target, and

one rotation to select the angle of incidence of the ions. As targets, thin layers of Pt evaporated onto carbon were used. The targets were kept at room temperature. On the targets no zinc condensation was detectable even after hours of measurement, within the detection limits of Rutherford backscattering (RBS), i.e., well below a monolayer. As RBS detector, a particle implanted silicon detector was used, mounted at an angle of  $90^\circ$  with respect to the incoming beam. Detector, preamplifier, and amplifier were operated at a constant temperature of  $0 \pm 0.1^\circ\text{C}$ , thus keeping thermal drifts sufficiently low so that the corresponding systematic error in the experiment was negligible.

### B. Gas phase stopping cross sections

Protons and deuterons in the energy range  $E_{\min} = 15$  keV/u to  $E_{\max} = 720$  keV/u were used as projectiles. The energy loss in the vapor cell was determined from the shift of the mean position of the peaks of the projectiles scattered in the platinum layer. At a fixed ion energy, the energy loss of the ions was measured for a number of vapor pressures determined via thermocouple readings. Care was taken to allow the system to reach thermal equilibrium. Thus, a typical measuring time for one energy is 2–3 h. Due to the high stability of the switching magnet, which defines the energy of the ion beam, this method is superior to the alternative keeping of the vapor pressure constant and varying the ion energy.

For a number of reasons, it seems impossible to obtain absolute numbers for the vapor density with an accuracy of 5%: Even if one eliminated (or took into account properly) the temperature gradient along the vapor cell, calibrated the thermocouples and corrected for the finite vapor pressure outside of the apertures, one would still be left with vapor pressure data which cannot be converted to pressure at the desired level of accuracy.<sup>15</sup> Furthermore, the charge equilibration at the entrance of the vapor cell would cause systematic errors if the energy-loss data  $\Delta E$  were evaluated versus the areal vapor densities  $n$ : To achieve charge-state equilibrium requires a characteristic length  $x_0$  (see Sec. III A). Depending on the ion velocity,  $x_0$  can amount up to 10% of the length of the gas cell. Therefore we decided to perform the energy-loss measurements as a *relative measurement*: We used thermocouples only to set certain temperatures  $T$ —and corresponding areal densities  $n$ —reproducibly to the same value for every ion energy  $E$ . Then, the slope of the linear regression of energy losses  $\Delta E(E, n)$  versus  $\Delta E(E_{\max}, n)$  at constant energy  $E$  yields the ratio of the stopping cross sections  $S_{\text{vap}}(E)/S_{\text{vap}}(E_{\max})$ . The reference value,  $S_{\text{vap}}(E_{\max})$ , has to be determined independently: We equate  $S_{\text{vap}}(E_{\max})$  to the theoretically calculated value at  $E_{\max}$  (see below). Thus, we obtain the stopping cross section in the gas phase at all energies. We stress that systematic errors in the conversion of the measured thermovoltages to vapor densities, due to temperature gradients along the vapor cell due to the effusion of zinc vapor or due to charge equilibration of the beam do not affect at all the slope of  $\Delta E(E, n)$  versus  $\Delta E(E_{\max}, n)$ , they just would affect the intercept. We find  $-0.3 \pm 0.2$

keV/u as a mean value of the intercepts. This is comparable to the statistical uncertainty of the data evaluation (0.2 keV), indicating that the influence of systematic errors on the slope is negligible. What remains is the statistical uncertainty of about 8% (standard deviation) of the measured data. The results obtained are shown in Fig. 2.

### C. Gas phase charge states

In order to measure the charge-state fractions  $\phi^+$  and  $\phi^0$  of protons and neutral hydrogen atoms, a magnetic deflection field was applied to the ion beam after exiting the vapor cell preventing the charged projectiles from hitting the scattering target. This measurement reflects the charge state of the projectiles inside the vapor cell; since no material different from the zinc vapor is exposed to the ion beam and, since there are no metastable states for hydrogen projectiles. The scattered intensities  $I_0$  and  $I_{\text{tot}}$  with and without applied magnetic field, respectively, were measured during equal times (100s) under stable current conditions. This yielded  $\phi^0 = I_0 / I_{\text{tot}}$ . At  $E_{\text{min}}$ , the charged beam intensities,  $I_+$  and  $I_-$ , were determined by displacing the scattering target while the magnetic field was applied. This resulted in  $\phi^- / \phi^+ = 0.15$ . Together with  $\phi^0(E_{\text{min}}) = 0.79$ , this yields  $\phi^+ = 0.18$  and  $\phi^- = 0.03$ , in agreement with similar measurements<sup>16</sup> at 15 keV/u. Due to the rapid decrease of  $\phi^-$  with increasing energy,  $\phi^-$  is less than 1% for all the higher energies  $E$  and is therefore negligible. Hence we assume  $\phi^+ = 1 - \phi^0$ . We find satisfactory agreement with Ref. 16 for  $E > 15$  keV/u. The data of Ref. 16 should be taken as lower bound values.<sup>17</sup> The statistical uncertainties of our data is at most 2%. In Fig. 3 we plot the measured charge-state distribution as a function of projectile energy.

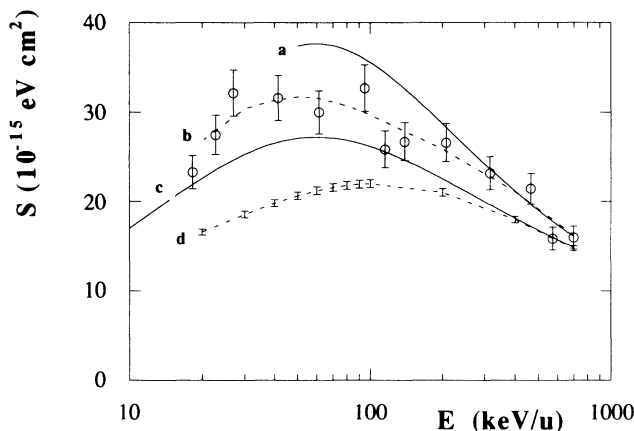


FIG. 2. Stopping cross section ( $10^{-15}$  eV  $\text{cm}^2$ ) for a H beam in Zn as a function of energy (keV/u). The dashed lines are the best fit to the measured data [curve (b) corresponds to the gas phase and (d) to the solid], and the solid curves are the calculated ones [curve (a) corresponds to the gas phase and (c) to the solid]. The dots are measured data for the gas, including an 8% error barr. The error barr in the solid data is only 2% and it is also indicated for some points in the figure.

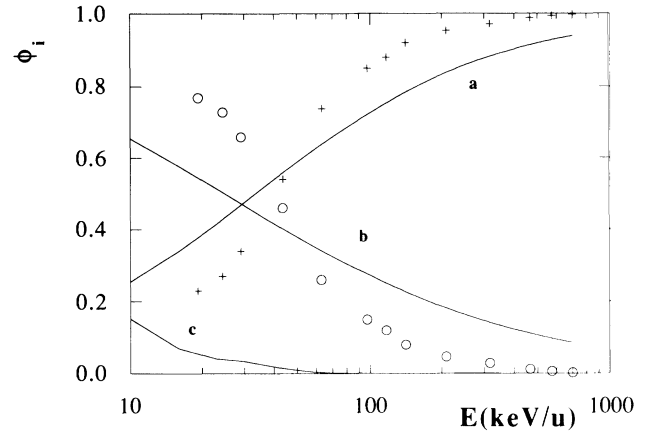


FIG. 3. Measured values for the equilibrium charge-state fractions  $\phi_i$  for protons (+) and hydrogen atoms (o) in the gas phase of Zn as a function of projectile energy (keV/u). Curves (a), (b), and (c) correspond to the calculated values for  $\phi^+$ ,  $\phi^0$ , and  $\phi^-$ , respectively in solid Zn, as obtained in our model.

### D. Solid phase

The stopping cross section for the solid phase was determined by the well-established Rutherford backscattering (RBS) technique:<sup>18</sup> Zinc was evaporated onto a carbon backing following Ref. 19; purity, stability under ion bombardment, and thickness homogeneity were checked by RBS. The stopping cross section was obtained<sup>18</sup> from the RBS spectra measured using protons and deuterons in the energy range 20–720 keV/u. The areal mass density of the zinc layer was measured relative to that of a copper target by applying charge collection and making use of the precisely known stopping cross section of copper for 500 keV/u hydrogen ions.<sup>20</sup> The uncertainty of the thickness determination amounts to  $\pm 5\%$ , while the statistical uncertainty of the stopping cross section measurements is at most  $\pm 2\%$ . These data are shown in Fig. 2 together with the theoretically calculated values for the two phases obtained using the model described in the following section.

## III. THEORY

### A. The charge-state approach

The energy loss of hydrogen projectiles in the solid and gas phase of zinc targets is obtained from a sum of partial stopping cross sections ( $S_i$ ) weighted with the corresponding charge-state fractions ( $\phi_i$ ).<sup>21</sup> For a charge equilibrated beam, the total stopping cross section is given by

$$S = \sum_i \phi_i (S_i^{el} + S_i^{in}), \quad (1)$$

where  $S_i^{el}$  is the contribution to the stopping cross section of charge-state fraction  $\phi_i$  due to target excitations associated with no change in the projectile state, while  $S_i^{in}$  is the one associated with changes in the projectile state.  $S_i^{in}$  includes, in principle, target excitation and ionization

associated with electron capture or projectile excitation and ionization. It is given by

$$S_i^{in} = \sum_{j,\alpha,\beta} W_{ij}(\alpha,\beta) \sigma_{ij}(\alpha,\beta), \quad \text{with } j \neq i \quad (2)$$

where  $\sigma_{ij}(\alpha,\beta)$  is the cross section for the excitation process in which the projectile state changes from  $i$  to  $j$  while the target state goes from  $\alpha$  to  $\beta$ .  $W_{ij}(\alpha,\beta)$  is the corresponding transition energy.

For a two-component system the characteristic length  $x_0$  to achieve charge-state equilibrium is given (from the solution of the rate equations) by

$$x_0 = \frac{1}{n(\sigma_c + \sigma_L)}, \quad (3)$$

where  $n$  is the target atomic density and  $\sigma_c(\sigma_L)$  are the capture (loss) cross section. The condition to be satisfied is that the target thickness  $L$  should be much larger than  $x_0$ . In the solid phase,  $n$  is so high that  $x_0$  is of the order of a few Å. In the gas phase, even though the density is about eight orders of magnitude lower, the actual length of the vapor cell ( $L=30$  cm) satisfies the required criterion [ $x_0/L < 0.1$ ].

The use of this capture and loss picture requires some justification in the case of the solid target because of its large density. If we define an inelastic mean free path  $\lambda$  from each of the total cross sections  $\sigma$  for the various channels by the relation

$$\lambda = \frac{1}{n\sigma}, \quad (4)$$

the condition to be satisfied is  $d < \lambda$ , where  $d$  is the lattice constant. Furthermore, the characteristic time scale  $\tau_p$  for the capture and loss processes is of the order of  $10^{-16}$  sec (the inverse plasma frequency  $\omega_p$  for valence electrons or typical time scale for inner shell capture), while the mean time between capture and loss events  $\tau_{C,L}$  is given by

$$\tau_{C,L} = \frac{1}{nv\sigma_{C,L}}, \quad (5)$$

where  $v$  is the ion speed and the other symbols have been

defined previously. The condition  $\tau_p \ll \tau_{C,L}$  ensures that capture and loss are independent events.

## B. Excitation spectra

The excitation spectrum of the zinc atom includes excitation and ionization of its thirty electrons in a  $[\text{Ar}]3d^{10}4s^2$  electronic structure. The  $4s \rightarrow 4p$  excitation is the dominant one at low energies.

In the condensed phase the outer shell electrons ( $3d$  and  $4s$ ) are those that change significantly their state as compared to the gas phase, giving rise to the band structure of Zn with all its interband and intraband transitions. However, solid-state electronic calculations<sup>22</sup> show that in the particular case of Zn the ten  $3d$  electrons are well below the Fermi level (around 10 eV) and retain a rather highly localized character,<sup>23</sup> while the two  $4s$  electrons build up a free-electron band. For this reason we have approximated the  $4s$  excitation of solid Zn by that of a free-electron gas with  $r_s=2.3$  (electron-hole pairs and plasmons), while ionization of the localized  $3d$  orbitals should end above the Fermi level. The lowest excitation for this system is the electron-hole pair creation. In Fig. 4 the energy levels of the two phases are depicted schematically.

## C. Methods

### 1. Target excitation

a. Gas phase. For the description of the Zn atomic state we have used a model potential approach based on the Hartree-Fock-Slater (HFS) potential  $V_{\text{HFS}}$  of the zinc ground state. This approach has been used by many authors in connection with energy-loss calculations and/or ionization processes.<sup>24</sup> The potential  $V_{\text{HFS}}$  can be extracted from the tables of Hermann and Skillmann<sup>25</sup> or from the program of Desclaux.<sup>26</sup> In this frame, the excited and continuum states of Zn are eigenstates of the Hamiltonian  $H_{\text{HFS}}$  for one electron moving in the potential  $V_{\text{HFS}}$ . We can check the accuracy of this approach by comparing the binding energy of the Rydberg states with the experimental value as given in the tables of Moore.<sup>27</sup> As we neglect spin-orbit forces, we compare

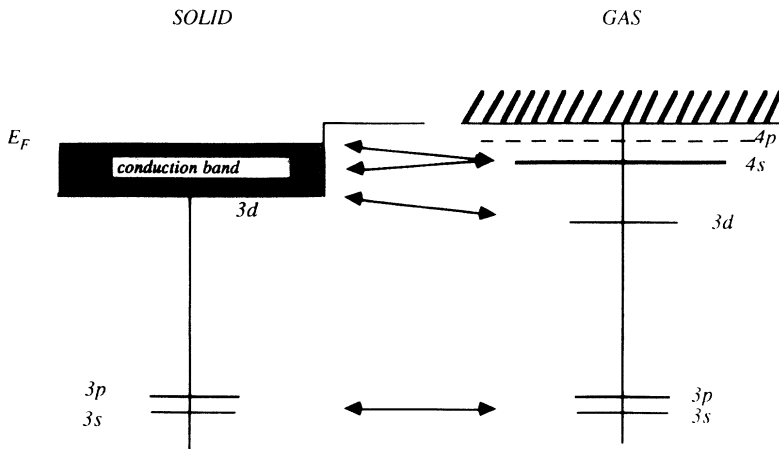


FIG. 4. Schematic representation of the zinc energy levels for the gas and solid.

the theoretical values with the weighted sum  $3E_T/4 + E_S/4$  of the triplet  $E_T$  and singlet  $E_S$  energies. The energy  $E_{nl}$  of the states in a Rydberg series with a given angular momentum  $l$  can be represented by the expression

$$E_{nl} = \frac{-1}{2(n - \mu_{nl})^2}, \quad (6)$$

where the quantum defect  $\mu_{nl}$  goes to the limit  $\mu_l$  as  $n$  goes to infinity. The theoretical values of  $\mu_l$  are 2.641 for  $l=0$ , 2.083 for  $l=1$ , 0.996 for  $l=2$ , and 2.9 (-4) for  $l=3$ . From Moore's table, we can extract  $\mu_{nl}$  for the largest available value of  $n$ . We get  $\mu_{9s}=2.7$ ,  $\mu_{9p}=2.17$ ,  $\mu_{7d}=1.12$ , and  $\mu_{5f}=0.03$ . The accuracy is therefore of the order of a few percent.

The bound and continuum eigenstates of  $H_{\text{HFS}}$  are determined numerically with the Numerov algorithm, and the target excitation and ionization cross section are determined with the first Born approximation (FBA).<sup>28</sup> In order to calculate the stopping cross section for a given initial state, one must sum over all final excited and continuum states. For excitation we have included in our evaluation  $s$ ,  $p$ ,  $d$ , and  $f$  excited states, the contribution from larger values of  $l$  being negligible. The Born excitation cross section was calculated for  $n$  up to 10 and then extrapolated using the expression

$$\sigma(nl) = \sigma(10l) \frac{(10 - \mu_l)^3}{(n - \mu_l)^3}. \quad (7)$$

We have checked that our results converge to the above expression with good precision.

For ionization, the partial wave expansion for a given electron energy has been truncated when the accuracy was better than  $10^{-3}$ . The stopping cross section was then determined by integration over electron energies. The theoretical value for 700 keV/u proton impact has been used for the normalization of the experiments and it has been determined with an accuracy of 1% (see Table I). The main source of error in this calculation comes from the evaluation of the energy loss connected with the neutral fraction of the beam (see the discussion below). In spite of the small neutral fraction, capture and projectile excitation contribute to 5% of the total energy loss at 700 keV/u.

For the case of  $H^0$  impact on zinc, we have calculated the target excitation assuming that the H atom is frozen in its ground state. In other terms, the interaction potential is the static potential of the H atom. This means that we have discarded all processes associated with a *simultaneous* projectile and target excitation. We discuss this problem in connection with projectile (H) excitation below.

b. Solid phase. The energy loss to target excitations for each of the projectile charge states has been calculated in a way similar to the gas phase calculations except for the  $4s$  electron excitations. The  $3s$  and  $3p$  contribution to the energy loss is taken as that due to ionization in the gas phase. For the contribution of  $3d$  ionization to the energy loss, we modify the energy levels according to

TABLE I. Energy loss for 700 keV/u protons ( $10^{-15}$  eV cm<sup>2</sup>). Contributions to the total stopping cross section of zinc in the gas phase for 700 keV/u protons. The calculated value is  $16.7 \times 10^{-15}$  eV cm<sup>2</sup> with 1% numerical accuracy.

Channel		Loss	Error
Ionization	4s	2.054	0.01
	3d	8.313	0.01
	3p	2.536	0.005
	3s	0.6651	0.0001
	2p	0.1708	0.0001
	2s	0.0531	0.0003
	Total	13.79	0.025
Excitation		2.10	
Capture and loss		0.785	0.15
Total		16.7	0.18

band-structure calculations and introduce a threshold for ionization at the Fermi level. We have used atomic wave functions for the  $3d$  electrons identical to those used for the gas phase. The continuum wave functions have also been described by eigenstates of  $V_{\text{HFS}}$ . This can be justified by the fact that our calculations depend on the part of the continuum functions which overlaps strongly with the  $3d$  orbital, i.e., the part close to the ion core. The relation between the electron energies  $E(k)$  and wave vector  $k$  has been taken as

$$E(k) = \frac{k^2}{2}, \quad (8)$$

where  $E(k)$  is the electron energy from the bottom of the band. Alternatively we have done a calculation using the HF relation for  $E(k)$  and found no significant difference. The projectile screening has been accounted for through an exponentially screened Coulomb potential with a screening parameter ( $\lambda$ ) that interpolates between the static ( $\lambda_0 = k_{\text{TF}}$ ) and high velocity limits ( $\lambda_\infty = \omega_p / v$ ) according to<sup>29</sup>

$$\frac{1}{\lambda^2} = \frac{1}{\lambda_0^2} + \frac{1}{\lambda_\infty^2}, \quad (9)$$

$k_{\text{TF}}$  is the Thomas-Fermi wave vector.

The  $4s$  electron contribution in our model is due to both electron-hole pairs and plasmons. As the latter are only excited at relatively high velocities we calculate its contribution to the proton energy loss using linear response theory for a unit charge.<sup>2</sup> However, the electron-hole pair excitation contribution to the energy loss is relevant at very low velocities where nonlinear effects are important.<sup>11</sup> So we evaluate the energy loss to electron-hole pair excitations from a full phase shift calculation of the transport cross section and integrating over relative velocities of the electron using different scattering potentials depending on the proton charge state<sup>29</sup> according to

$$\frac{dE}{dx}(v) = \frac{1}{4\pi^2} \frac{1}{v^2} \int_0^{v_F} u \, du \int_{|v-u|}^{v+u} dv_r v_r^4 \sigma^{\text{tr}}(v_r) \times \left[ 1 + \frac{v^2 - u^2}{v_r^2} \right], \quad (10)$$

where  $\sigma^{\text{tr}}$  is the transport cross section. For the  $\text{H}^+$  charge state we use a linearly screened potential for a point charge ( $\text{H}^+$ ) and for  $\text{H}^0$  we take into account the electron charge density in the 1s state ( $\text{H}^0$ ) with a simple Thomas-Fermi dielectric function [the screening parameter  $\lambda$  varying according to the above mentioned law, i.e., Eq. (9)]. For the  $\text{H}^-$  charge state we use the density functional result for the self-consistent screened potential to calculate the low velocity stopping from the transport cross section at the Fermi level.<sup>30</sup>

## 2. Electron capture

a. Gas phase. Energy loss in capture processes by proton is calculated from the continuum distorted-wave (CDW) capture cross sections with a proper treatment of the statistics. The CDW method can be derived as the first order of a perturbative treatment which accounts correctly for Coulomb asymptotic conditions.<sup>31</sup> The perturbative nature of the approximation limits its applicability to low energies. In practice, it has been found to be valid for energies larger than 80 keV/u times the initial or final binding energy expressed in atomic units. In the present case, capture by protons takes place mainly from the 3d shell of Zn and therefore the CDW approximation should be valid according to this criterion, above 50 keV/u. This criterion elaborated from studies on light targets, is too optimistic. In the present instance where the 3d shell contains ten electrons, we have checked that the CDW calculations give capture probabilities much larger than one for small impact parameters. We have therefore corrected the CDW calculations in the following way. Let  $p_i$  ( $i=1, \dots, 4$ ) be the probability of capturing one electron from the subshells 4s, 3d<sup>0</sup>, 3d<sup>1</sup>, and 3d<sup>2</sup>, respectively for a given impact parameter. We define the capture probability as

$$P_c = \sum_i n_i p_i \frac{P}{(1-p_i)}, \quad P = \prod_i (1-p_i)^{n_i}, \quad (11)$$

where  $n_i$  is the number of electrons in each shell. Whenever one of the  $p_i$  becomes larger than one we take either  $P_c = 0$  or  $P_c = 1$ . As this takes place only at small impact parameters, the difference between the two calculations is not large, amounting to 25% at 50 keV/u and 15% at 100 keV/u. Equation (11) is exact when  $p_i \ll 1$ . In sum, our conclusion is that, though the CDW method is not fully reliable between 50 and 100 keV/u, it can be used safely to gauge the energy loss associated with capture as well as its role in the phase effect.

b. Solid phase. The cross section for 3d electron capture is calculated in the CDW approximation as if it were an atomic-type process. The only solid-state effects taken into account are the shift in the energy levels both for target and projectile electrons and the modification in the electron wave function due to screening for the bound

state around the proton according to the model of Guinea, Flores, and Echenique.<sup>8,32</sup>

An electron from the conduction band (4s) may be captured by the moving proton due to the screened electron-electron interaction in a three-body recombination process (TBRP).<sup>11</sup> At zero velocity these processes correspond to the well-known Auger capture processes. We calculate the corresponding cross section in first-order time dependent perturbation theory.<sup>32</sup>

## 3. Projectile excitation

a. Gas phase. It is a difficult problem *per se*. As the H atom experiences a strong potential close to the target Zn cores, perturbation theory is not valid. On the other hand the neutral fraction is known for the gas phase from the measurements. We have therefore evaluated the energy loss in the following way. From the total capture cross section and the measured charge-state fractions we obtain the total projectile electron loss cross section. The energy lost in this process is then approximated by this loss cross section times the FBA mean transition energies. The latter is calculated for  $\text{H}^0$  interaction with the frozen Zn atom. Let us define the mean excitation energy by projectile electron capture ( $E_C$ ) and loss ( $E_L$ ) as

$$S_C = \sigma_C E_C \quad \text{and} \quad S_L = \sigma_L E_L, \quad (12)$$

where  $\sigma_C$  and  $\sigma_L$  are the total capture and loss cross sections, while  $S_C$  and  $S_L$  are the stopping cross sections in capture and loss, respectively. Neglecting projectile excitation the total energy loss in capture and loss processes by the projectile is

$$S_{C\&L} = \frac{\sigma_C}{\sigma_C + \sigma_L} \sigma_L E_L + \frac{\sigma_L}{\sigma_C + \sigma_L} \sigma_C E_C = \phi^+ \sigma_C (E_C + E_L), \quad (13)$$

where  $\phi^+$  is the fraction of protons. So, if the fraction of protons and the capture cross sections are known, we only need  $E_L$  to calculate the contribution of electron loss by the projectile to the total energy loss. The latter quantity is more sensitive to the *range* of the potential than to its absolute magnitude. By doing various calculations in which we cut down arbitrarily the short-range part of the static potential of Zn, we find that  $E_L$  does not vary by more than 50%, whereas, under the same condition the cross section varies by orders of magnitude. We have therefore used for  $E_L$  the value given by the Born approximation for the ionization of H by the static potential of Zn. This problem is still relevant at 700 keV/u, where we normalize the experiment to theory. For this high-energy  $\phi^+$  is close to unity and  $S_{C\&L} \cong \sigma_C (E_C + E_L)$ . We get 380 eV for  $E_C$  and 230 eV for  $E_L$ . As  $S_C$  is equal to  $4.9 \times 10^{-16}$  eV cm<sup>2</sup>, we estimate the error in the total energy loss to be of the order of 1% (corresponding to a 50% error in  $E_L$  which is overestimated).

b. Solid phase. At typical metallic densities ( $2 < r_s < 5$ ) the screening by the conduction-band electrons is not strong enough to avoid the appearance of bound states around the proton.<sup>33</sup> Effects due to the interaction with

the lattice ion cores would reduce the lifetime of this bound states as the ion velocity increases but at the same time screening is less and less effective. One could think of these bound states around the proton as resonances with a finite lifetime (given by the loss cross section). We use the model of Guinea, Flores, and Echenique<sup>8,32</sup> to describe the charge states of protons in an electron gas. The wave function and binding energy are calculated by minimizing the total energy of the system using a variational procedure. Account is also taken of the dynamic screening of the interaction by the conduction-band ( $4s$ ) electrons.

Due to screening, only one bound state around the proton exists. Electron loss by the projectile is taken into account by two different mechanisms: the interaction with the lattice ion cores and the interaction with the electron gas. Both cross sections are calculated in first-order time dependent perturbation theory using different interaction potentials (both of them are supposed to be weak). For the interaction with the lattice ion cores we use a screened Ashcroft pseudopotential<sup>34</sup> to describe the interaction between the bound electron and the lattice ions. This is a reasonable approximation for low-energy electrons. For the interaction with the electron gas we use the dynamically screened interaction according to the model of Guinea, Flores, and Echenique. This is the inverse of the TRBP mentioned above Sec. II C 2.

#### IV. RESULTS

##### A. $4s$ excitation

In Fig. 5 we plot the partial stopping cross section from  $4s$  excitation by  $H^+$  and  $H^0$  projectiles as a function of projectile energy for the two phases. By comparing curves (a) and (b) one can see that below 100 keV/u the  $4s$  electron excitation by  $H^+$  impact is much larger in the gas phase and it is more than two times that of the solid

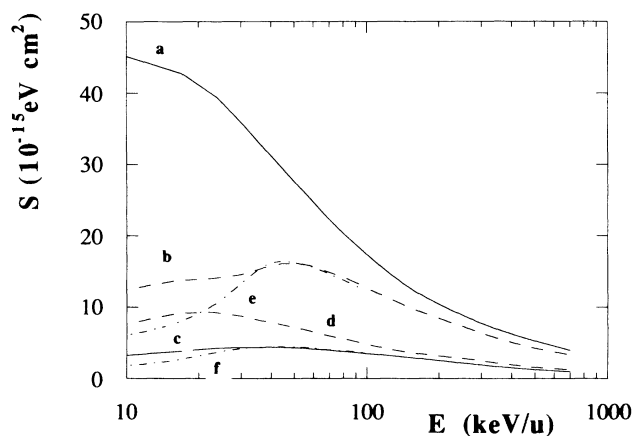


FIG. 5. Stopping cross section from  $4s$  excitation. Curve (a) and (b) correspond to  $H^+$  projectiles in the gas and solid phase, respectively, and curve (e) is the result of a first Born calculation (linear screening in the dielectric formalism) for the solid. Curves (c) and (d) are the corresponding ones for  $H^0$  projectiles in the gas and solid phase, and curve (f) is the first Born result for  $H^0$  in the solid (see the text).

phase below 20 keV/u. This difference does not come out of nonlinear effects, included in the calculations for the solid case. A first Born calculation for proton stopping in the solid phase (linear screening in the dielectric formalism) given as curve (e) shows essentially the same difference with respect to the gas phase.

The main reason that explains the difference is the long-range Coulomb interaction between the proton and the  $4s$  electrons in the Zn atom as compared to the short-range interaction due to screening in the solid phase. This means that even though mean transition energies (defined as the ratio of the stopping cross section to the cross section) are about the same or a little bit larger for the solid (of the order of 10 eV for the two phases for 20 keV/u protons) the transition probabilities are much larger in the gas phase, where the dipole transition  $4s \rightarrow 4p$  has the largest weight in the low-energy excitation spectrum. The relative contribution of the  $4s \rightarrow 4p$  transition to the energy loss by excitation of the  $4s$  orbital is 50% at 10 keV/u and 40% at 700 keV/u in spite of the small value of the transition energy (4.6 eV). This transition corresponds to a long-range dipolar interaction which decreases slowly with impact parameter [see Fig. 6]. Incidentally, it is the long-range behavior which justifies the use of a Born approximation even for the low impact energies of interest in this work.

The property that introduces the most remarkable phase effect is the strong polarizability of the  $4s$  valence band: It shields the projectile potential and reduces the range of the projectile interactions. The screening is strongest in the static limit and becomes small and amenable to a perturbation treatment at high velocities  $v \gg v_F$ .

The three curves [(a), (b), and (e)] merge at high ener-

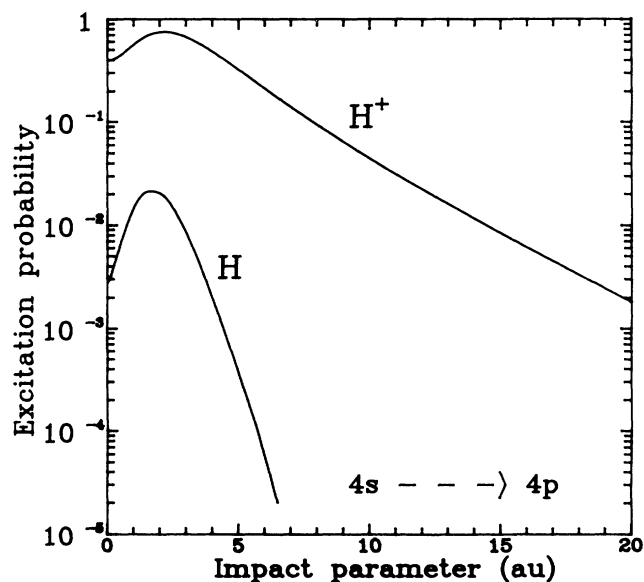


FIG. 6. Excitation probability as a function of impact parameter (in atomic units) for the  $4s \rightarrow 4p$  transition in the gas phase. The figure shows the strong reduction of the interaction due to screening by the bound electron in the case of  $H^0$  impact. The projectile energy is  $E = 50$  keV/u.

gies, as they should, though coming from completely different calculations. This shows that binding and solid-state effects are not so crucial for high-energy collisions as compared to the low-energy case.

On the other hand the  $H^0$  stopping in the two phases is not that different [curves (c) and (d)] due to the efficient screening by the projectile bound electron that strongly suppresses the  $4s \rightarrow 4p$  excitation in the gas phase. Curve (f) corresponds to a first Born calculation (linear screening in the dielectric formalism) for  $H^0$  stopping in the solid phase and shows a remarkable difference (around a factor of 2 smaller) with the nonlinear screening calculation shown as curve (d). Curve (f) is the equivalent to curve (e) for the bare proton case; the difference is that for the  $H^0$  atom account is taken for the electron cloud around the nucleus.<sup>35</sup>

Furthermore, the difference between  $H^0$  and  $H^+$  stopping due to  $4s$  electron excitation is very large in the gas phase. Comparing curves (a) and (c) one sees that this difference may be up to a factor of 10 at low energies corresponding to a decrease of the excitation loss by a factor of at least 30. This difference is due to the  $4s-4p$  transition: The long-range dipolar interaction is quenched in the case of  $H^0$  projectiles. However, in the solid phase [curves (b) and (d)], the difference is much smaller, especially at low energies ( $\cong 50$  keV/u). As a consequence an accurate determination of the charge-state distribution in the gas phase is required but not in the solid phase to explain the part of the phase effect due to  $4s$  electron excitations.

### B. $3d$ excitations

In Fig. 7 we plot the partial stopping cross sections from  $3d$  electron excitations by  $H^+$  and  $H^0$  impact for the two phases. Comparison between the curves (a) and (b), that correspond to an  $H^+$  projectile in the gas and solid, respectively, shows that  $3d$  excitations give only a slight difference between the phases, and so a small contribution to the phase effect, which is more noticeable at higher energies where its relative contribution to the total

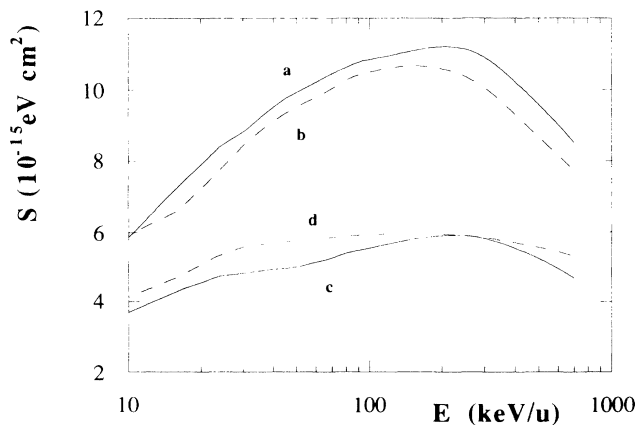


FIG. 7. Stopping cross section from  $3d$  excitation. Curve (a) and (b) correspond to  $H^+$  projectiles in the gas and solid phase, respectively. Curves (c) and (d) are the corresponding ones for  $H^0$  projectiles in the gas and solid phases.

stopping cross section is larger [see Fig. 10]. Similar conclusions can be drawn analyzing curves (c) and (d) that correspond to an  $H^0$  projectile.

### C. Electron capture

The contribution to the stopping cross section of the  $H^+$  charge state from electron capture processes is shown in Fig. 8. At high energies ( $E > 200$  keV/u) it is about the same for the two phases, but at low energies ( $E < 100$  keV/u) capture processes in the gas phase contribute up to twice the solid phase. This is mainly due to the fact that, even though capture cross section are very similar (except at very low energies where  $4s$  electron capture dominates), the transition energies are much larger in the gas phase. The different relative positions of the target and projectile electron energy levels is an important effect at low energies. The  $3d$  electron binding energy in the Zn atom is about 20 eV and the hydrogen level lies 13.6 eV below vacuum giving a transition energy in the capture process for a collision at relative velocity  $v$  which is  $\Delta\epsilon_{\text{gas}} = 6.4 \text{ eV} + v^2/2$ . On the other hand, the  $3d$  electrons in the solid are at the bottom of the conduction band and the hydrogen level too, so in the solid  $\Delta\epsilon_{\text{solid}} \cong v^2/2$ . At low velocities the difference is important but at high energies ( $E > 200$  keV/u) there is essentially no difference: At high energies, binding effects are not important and only the high momentum components of the target and projectile wave functions are relevant and so one would not expect any difference between the gas and solid phases.

### D. Projectile excitation

The contribution to the stopping cross section of  $H^0$  due to projectile ionization (electron loss) is shown in Fig. 9. It is obviously another source for the phase effect in the energy range  $50 < E < 700$  keV/u. As we discussed before, in Sec. III C 3, the loss cross section in the gas phase has been probably overestimated, while the opposite is true for the solid, at high energies. This is the reason why the contribution to the stopping cross section

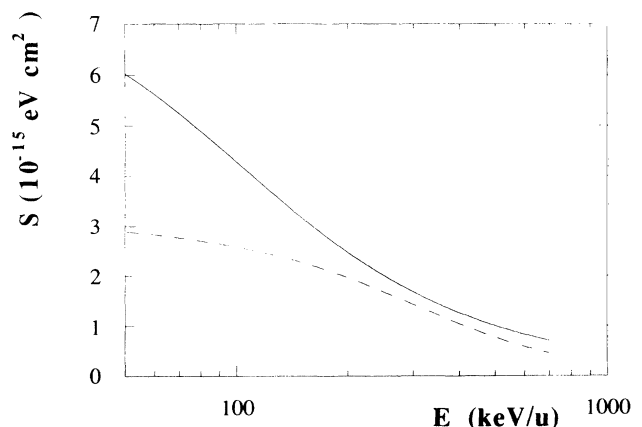


FIG. 8. Stopping cross section from capture processes. The solid line is the gas phase result and the dashed line corresponds to the solid.

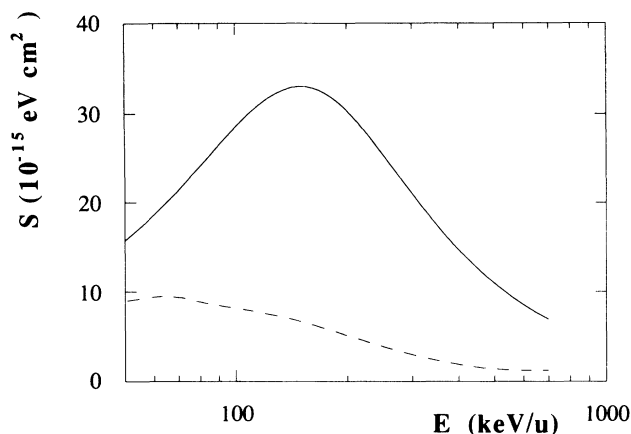


FIG. 9. Stopping cross section from loss processes (projectile ionization). The solid line is the gas phase result and the dashed line corresponds to the solid.

of the  $H^0$  charge state from projectile excitation is so different at high energies. More precisely, in the solid phase the use of an Ashcroft pseudopotential may be adequate up to 100 keV/u energies ( $v = 2v_0$ , where  $v_0$  is the Bohr velocity) but it is probably not so adequate at high energies where the projectile electron sees the core of the atoms. In the gas phase the loss cross section is obtained from the measured charge-state fractions and the calculated capture cross section. But the mean transition energies are obtained from a first Born calculation that may be off by as much as a factor of 2. Altogether these effects may explain the discrepancy between the two curves in the high-energy side. Anyhow, one has to remember that this charge-state fraction is minority at energies  $E > 200$  keV/u in both phases [see Fig. 3].

#### E. Charge-state distributions

The equilibrium charge-state distributions, shown in Fig. 3, which we calculate for the solid phase are quite different from the measured ones for the gas phase, showing on average a lower charge state. This reflects the fact that, even though capture cross sections are not too different, loss cross sections are strongly reduced in the solid phase as compared to the gas phase, mainly at low energies. This is partially due to the Pauli exclusion principle that prevents projectile ionization to continuum states below the Fermi level giving rise to an effective threshold (the bandwidth plus the binding energy) at low energies for this process.<sup>36</sup>

Since the  $H^+$  fraction has a steep growth at  $E \cong 50$  keV/u, we may expect the existence of a maximum in the phase effect in the energy range  $50 < E < 100$  keV/u; the large difference in stopping between gas and solid at low energies will be strongly reduced by the low fraction of  $H^+$  projectiles in both phases at those energies.

#### F. Relative contributions to the phase effect

In Fig. 10 we plot the different contributions to the phase effect, defined as the difference between the gas phase and solid phase stopping cross section

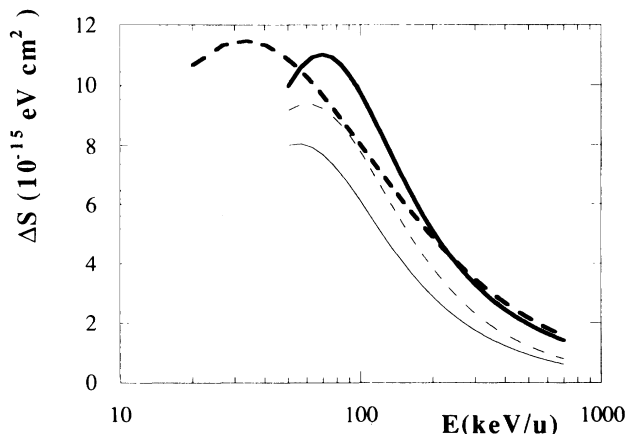


FIG. 10. Phase effect as a function of projectile energy (see the text for the definition of  $\Delta S$ ). The thick solid line corresponds to the calculated value and the thick dashed line to the measured one. The thin solid line gives the contribution to  $\Delta S$  from  $H^+$  excitation of the  $4s$  shell. The latter contribution plus that of  $H^0$  ionization is given as the thin dashed line.

[ $\Delta S = S_{\text{gas}} - S_{\text{sol}}$ ], as a function of projectile energy. The agreement between theory and experiment is quite good even though theoretical values always overestimate the measured ones (see Fig. 2).

Our model explains this difference as coming mainly from the different  $4s$  excitation by protons in the two phases and by projectile ionization up to energies of the order of 100 keV/u. At higher energies projectile ionization is not so important and both  $4s$  and  $3d$  excitation by protons give an appreciable contribution to the phase effect (see Figs. 5 and 7), being about  $1.5 \times 10^{-15}$  eV cm<sup>2</sup> for 700 keV/u protons.

#### V. CONCLUSION

We have found that the stopping cross section of atomic Zn for 50 keV/u H projectiles is about 1.5 times larger than that of solid Zn. The difference decreases for increasing energies and amounts to 14% at 700 keV/u.

We conclude that the explanation of the phase effect in H-Zn collisions is simple: The most important mechanism is the dynamic screening of the proton in the solid phase. As a consequence the projectile-target interaction is of shorter range for the solid as compared to the gas target. This effect is more noticeable for the outer shell electron excitation (valence electrons in the solid and  $4s$  electrons in the gas). A byproduct of the screening effect is that excitation by  $H^+$  and  $H^0$  are very similar, even for the valence electrons, in the solid but not at all in the gas.

We then expect a large phase effect for those elements in which the outer shell electrons are weakly bound in the atom and present delocalized valence electrons in the solid phase participating in the screening.

#### ACKNOWLEDGMENTS

The authors gratefully acknowledge help and financial support by Ministerio de Educación y Ciencia no. de Proyecto PB92-0474, Euskal Herriko Unibertsitatea, Gipuz-

koako Foru Aldundia, Eusko Jaurlaritza, and Iberdrola S. A. We are indebted to M. Peñalba for her help in the numerical calculations and to Eugene McGuire for sending us results of a first Born calculation for proton stopping in the gas phase of Zn which was very useful for starting this work. One of us (A.S.) has been partially supported by the Conseil Regional d'Aquitaine. The experimental part was partially supported by the Jubiläumsfonds of the Österr. Nationalbank. The help

of Chr. Eppacher in performing some of the RBS experiments is gratefully acknowledged. The cooperation between the groups in San Sebastian and Linz was facilitated by the Spanish Ministerio de Asuntos Exteriores and the Österr. Ministerium für Wissenschaft und Forschung. One of us (P.B.) would like to express his gratitude for the kind hospitality of the Departamento de Física de Materiales of the Universidad del País Vasco in San Sebastian.

- <sup>1</sup>H. Bethe, *Ann. Phys. (Leipzig)* **5**, 325 (1930).  
<sup>2</sup>J. Lindhard, K. Dan. Vidensk. Selsk. Mat. Fys. Medd. **28**, No. 8 (1954).  
<sup>3</sup>J. Ziegler, *Handbook of Stopping Cross Sections for all Elements* (Pergamon, New York, 1980).  
<sup>4</sup>D. I. Thwaites, *Nucl. Instrum. Methods B* **12**, 84 (1985).  
<sup>5</sup>P. Bauer, W. Rössler, and P. Mertens, *Nucl. Instrum. Methods B* **69**, 46 (1992).  
<sup>6</sup>J. R. Sabin and J. Oddershede, *Nucl. Instrum. Methods B* **36**, 249 (1989).  
<sup>7</sup>D. I. Thwaites, *Nucl. Instrum. Methods B* **69**, 53 (1992).  
<sup>8</sup>F. Guinea, F. Flores, and P. M. Echenique, *Phys. Rev. Lett.* **47**, 245 (1981).  
<sup>9</sup>S. Kreussler, C. Varelas, and W. Brandt, *Phys. Rev. B* **23**, 82 (1981); W. Brandt and M. Kitagawa, *ibid.* **25**, 5631 (1982).  
<sup>10</sup>W. Meckbach and S. K. Allison, *Phys. Rev.* **132**, 294 (1963).  
<sup>11</sup>P. M. Echenique, F. Flores, and R. H. Ritchie, in *Solid State Physics: Advances in Research and Applications*, edited by H. Ehrenreich (Academic, New York, 1990), Vol. 43, p. 229.  
<sup>12</sup>P. Bauer, F. Kastner, A. Arnau, A. Salin, P. D. Fainstein, V. H. Ponce, and P. M. Echenique, *Phys. Rev. Lett.* **69**, 1137 (1992).  
<sup>13</sup>A. G. Gaydon, *Dissociation Energies and Spectra of Diatomic Molecules* (Chapman and Hall, London, 1947).  
<sup>14</sup>C. Mitterschiffthaler and P. Bauer, *Nucl. Instrum. Methods B* **36**, 249 (1989).  
<sup>15</sup>K. Schäfer and E. Lax, *Eigenschaften der Materie in ihren Aggregatzuständen 2. Teil* (Springer-Verlag, Berlin, 1967).  
<sup>16</sup>B. A. Dyachkov and V. I. Zinenko, *At. Energ.* **24**, 18 (1968) [*Sov. At. Energy* **24**, 16 (1968)].  
<sup>17</sup>T. L. Morgan, R. E. Olson, A. S. Schalachter, and J. W. Gal-  
lager (unpublished).  
<sup>18</sup>C. Eppacher and D. Semrad, *Nucl. Instrum. Methods B* **35**, 109 (1988).  
<sup>19</sup>H. J. Maier, H. U. Friebel, D. Frischke, and R. Grossmann, *Nucl. Instrum. Methods A* **282**, 128 (1989).  
<sup>20</sup>H. Paul, D. Semrad, and A. Seilinger, *Nucl. Instrum. Methods B* **61**, 261 (1991).  
<sup>21</sup>A. Dalgarno and G. W. Griffing, *Proc. Phys. Soc. London, Sect. A* **66**, 961 (1953); **67**, 663 (1954); S. K. Allison, J. Cuevas, and M. García Muñoz, *Phys. Rev.* **127**, 792 (1962); A. Arnau, M. Peñalba, P. M. Echenique, and F. Flores, *Nucl. Instrum. Methods B* **69**, 102 (1992).  
<sup>22</sup>V. L. Moruzzi, J. F. Janak, and A. R. Williams, *Calculated Electronic Properties of Metals* (Pergamon, New York, 1978).  
<sup>23</sup>A. R. Williams and U. von Barth, in *Theory of the Inhomogeneous Electron Gas*, edited by S. Lundqvist and N. H. March (Plenum, New York, 1983), p. 291.  
<sup>24</sup>D. H. Madison, *Phys. Rev. A* **8**, 2449 (1973); E. J. McGuire, *ibid.* **26**, 1858 (1982); N. M. Kabachnik, *Nucl. Instrum. Methods B* **69**, 76 (1992).  
<sup>25</sup>F. Herman and S. Skillmann, *Atomic Structure Calculations* (Prentice Hall, Englewood Cliffs, NJ, 1963).  
<sup>26</sup>J. P. Desclaux, *Comput. Phys. Commun.* **1**, 216 (1969).  
<sup>27</sup>C. F. Moore, *Atomic Energy Levels* (NBS, Washington, 1971).  
<sup>28</sup>M. R. C. McDowell and J. P. Coleman, *Introduction to the Theory of Ion-Atom Collisions* (North-Holland, Amsterdam, 1970).  
<sup>29</sup>M. Peñalba, A. Arnau, P. M. Echenique, F. Flores, and R. H. Ritchie, *Europhys. Lett.* **19**, 45 (1992).  
<sup>30</sup>P. M. Echenique, R. Nieminen, and R. H. Ritchie, *Solid State Commun.* **37**, 779 (1981).  
<sup>31</sup>I. M. Cheshire, *Proc. Phys. Soc.* **84**, 89 (1964); Dz. Belkic, R. Gayet, and A. Salin, *Phys. Rep.* **56**, 279 (1979); *Computer Phys. Commun.* **32**, 385 (1983).  
<sup>32</sup>F. Guinea, F. Flores, and P. M. Echenique, *Phys. Rev. B* **25**, 6209 (1982).  
<sup>33</sup>B. Vinter, *Phys. Rev. B* **17**, 2429 (1978); J. K. Norskov, *ibid.* **17**, 446 (1978).  
<sup>34</sup>V. Heine, in *Solid State Physics*, edited by H. Ehrenreich, F. Seitz, and D. Turnbull (Academic, New York, 1970), Vol. 24, p. 186.  
<sup>35</sup>A. Arnau and P. M. Echenique, *Nucl. Instrum. Methods B* **42**, 165 (1989).  
<sup>36</sup>P. M. Echenique and F. Flores, *Phys. Rev. B* **35**, 8249 (1987).

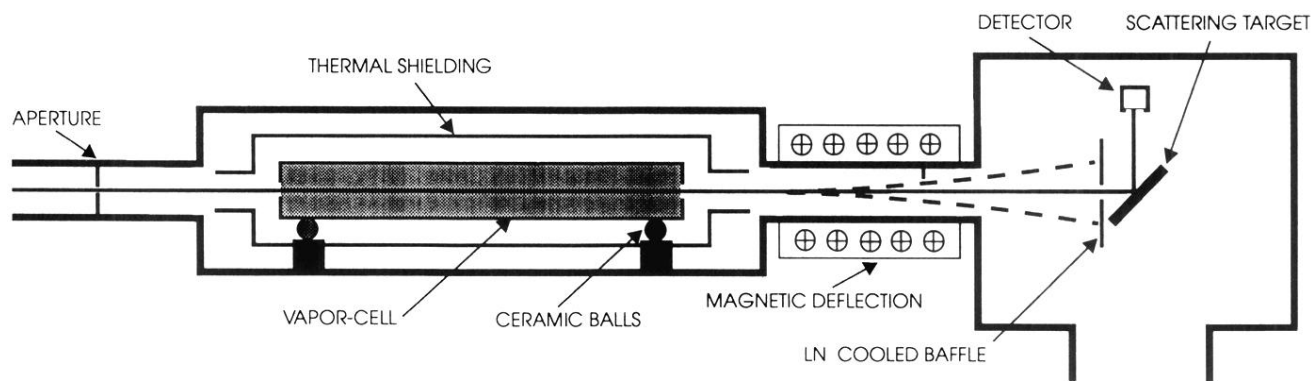


FIG. 1. Schematic representation of the experimental setup.

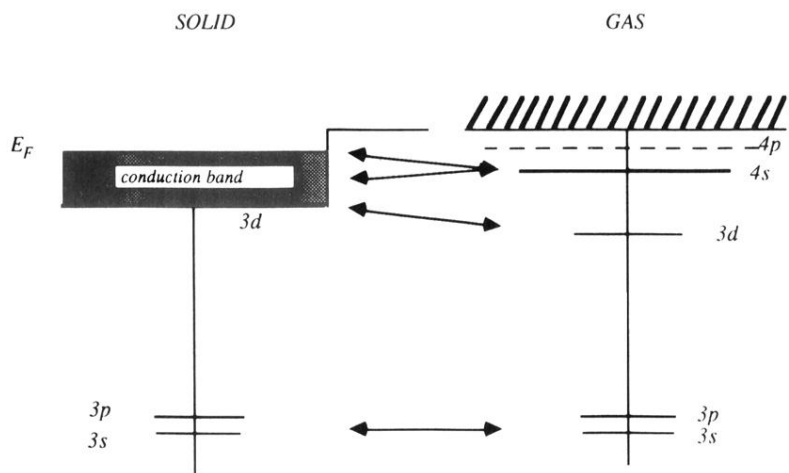


FIG. 4. Schematic representation of the zinc energy levels for the gas and solid.